Synchronization transitions in coupled time-delay electronic circuits with a threshold nonlinearity

K. Srinivasan[1], D. V. Senthilkumar[2,3], K. Murali[4], M. Lakshmanan[1], and J. Kurths[3,5]

[1]*Centre for Nonlinear Dynamics, Department of Physics,*
Bharathidasan University, Tiruchirapalli-620024, India
[2]*Centre for Dynamics of Complex Systems,*
University of Potsdam, 14469 Potsdam, Germany
[3]*Potsdam Institute for Climate Impact Research,*
14473 Potsdam, Germany
[4]*Department of Physics,*
Anna University, Chennai, India
[5]*Institute of Physics, Humboldt University,*
12489 Berlin, Germany

Experimental observations of typical kinds of synchronization transitions are reported in unidirectionally coupled time-delay electronic circuits with a threshold nonlinearity and two time delays, namely feedback delay τ_1 and coupling delay τ_2. We have observed transitions from anticipatory to lag via complete synchronization and their inverse counterparts with excitatory and inhibitory couplings, respectively, as a function of the coupling delay τ_2. The anticipating and lag times depend on the difference between the feedback and the coupling delays. A single stability condition for all the different types of synchronization is found to be valid as the stability condition is independent of both the delays. Further, the existence of different kinds of synchronizations observed experimentally is corroborated by numerical simulations, and from the changes in the Lyapunov exponents of the coupled time-delay systems.

PACS numbers: 05.45.Xt,05.45.Pq

I. INTRODUCTION

Time-delay is a veritable blackbox which can give rise to several interesting and novel phenomena such as multistable states [1], amplitude death [2], chimera states [3], phase flip bifurcation [4], Neimark-Sacker type bifurcations [5], etc., which cannot be observed in the absence of delay in the underlying systems. Further, it has also been shown that delay coupling in complex networks enhances the synchronizability of networks and interestingly it leads to the emergence of a wide range of new collective behavior [5, 6]. On the other hand, it has also been shown that connection delays can actually be conducive to synchronization so that it is possible for delayed systems to synchronize, whereas the undelayed systems do not [5]. Enhancement of neural synchrony, that is, the existence of a stable synchronized state even for a very low coupling strength for a significant time-delay in the coupling has also been demonstrated [7]. Time-delay feedback has been used to generate high-dimensional, high-capacity waveforms at high bandwidths to sucessfully transfer digital information at gigabit rates by chaotically fluctuating laser light travelling over 120 kilometers of a commercial fibre-optic link around Athens, Greece [8]. Time-delay feedback control has also been used to control pattern formation in neuroscience to prevent the pathological activity in cortical tissues [9, 10].

Synchronization in dynamical systems with time-delay feedback and in intrinsic time-delay systems with/without time-delay coupling has been receiving cen-

tral importance during the past decade both theoretically and experimentally [5–28]. However, experimental investigations/confirmations of theoretical results of synchronization transitions in coupled time-delay systems remain lagging in the available literature. Nevertheless, experimental investigations on differerent kinds of synchronization transitions in semiconductor laser systems with a delay feedback have been carried out recently [5–21]. However, experimental investigations in intrinsic time-delay systems, whose dynamics cannot be realized in the absence of time-delay such as the paradigmatic Mackey-Glass or Ikeda systems, using electronic circuits remain poorly explored and very few experimental results have been reported so far [22–25].

In particular, real time anticipatory synchronization of chaotic states using time-delayed electronic circuits with single-humped smooth nonlinearity was demonstrated by Voss [22]. Dual synchronization of chaos in two pairs of unidirectionally coupled Mackey-Glass electronic circuits with time-delayed feedback was demonstrated in [23]. These authors have also investigated the regions for achieving dual synchronization of chaos when the delay time is mismatched between the drive and response circuits. The effect of frequency bandwidth limitations in communication channels on the synchronization of two unidirectionally coupled Mackey-Glass analog circuits was demonstrated in [24]. Recently, experimental demonstration of simultaneous bidirectional communication between two chaotic systems by means of isochronal synchronization was carried out using Mackey-Glass elec-
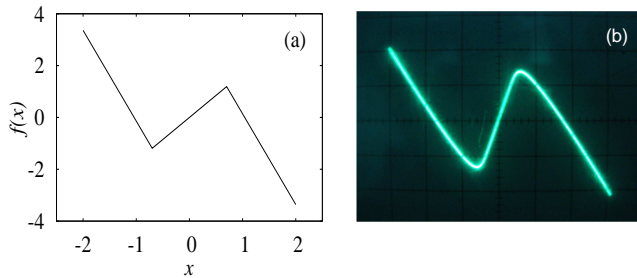
FIG. 1: (Colour online) The nonlinear function $f(x)$. (a) Plot of the piecewise linear function $f(x)$ given by Eq. (1). (b) Measured characteristic curve of the nonlinear unit ND from Fig. 3, U_{in}vsU_{out}. Vertical scale $2V/div$., horizontal scale $1V/div$.

FIG. 2: Circuit block diagram of the delayed feedback oscillator with a nonlinear device unit (ND), a time delay unit (DELAY) and a lowpass first-order R_0C_0 filter. $U(t)$ is the voltage across the capacitor C_0 and $U(t - T_d)$ is the voltage across the delay unit (DELAY).

tronic circuits with time-delay feedback [25].

Further, experimental observation of both anticipated and retarded synchronization has been demonstrated using unidirectionally coupled semiconductor lasers with delayed optoelectronic feedback [21]. It has been shown that depending on the difference between the transmission time and the feedback delay time the lasers fall into either anticipated or retarded synchronization regimes, where the driven receiver laser leads or lags behind the driving transmitter laser, confirming the theoretical works of Voss and Masoller [29–31]. Recently, we have demonstrated theoretically the transition from anticipatory to lag via complete synchronization as a function of the coupling delay with suitable stability condition in a system of unidirectionally coupled time-delay systems [27]. Further, it was also shown that anticipatory/lag synchronizations can be characterized using appropriate similarity functions and the transitions from a desynchronized state to an approximate anticipatory/lag synchronized state is characterized by a transition from on-off intermittency to periodicity in the laminar phase distribution settling the skepticism on characterizing anticipatory/lag synchronization using the similarity function as discussed by Zhan etal [32].

In the present manuscript, we will demonstrate experimentally all the aforesaid synchronization transitions, along with their inverse counterparts with inhibitory coupling, in a unidirectionally coupled time-delay electronic circuit with a threshold nonlinearity supported by an appropriate theoretical analysis. Specifically, in this manuscript we demonstrate the transition from anticipatory to complete and then from complete to lag synchronizations as a function of the coupling delay, for a fixed set of other system parameters, in a unidirectionally coupled piece-wise linear (designed using a threshold controller) time-delay electronic circuit. Further we will also show the existence of their inverse counterparts, that is the transition from inverse anticipatory to inverse lag synchronizations via inverse complete synchronization, with inhibitory coupling. The importance of inhibitory coupling and its intrinsic role in neural synchrony are dis-
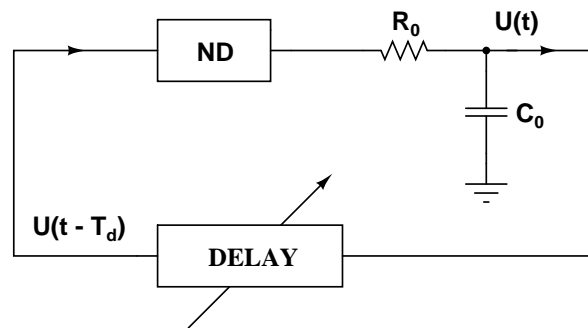
cussed in [28, 33, 34]. Furthermore, we will also show that neither inverse complete synchronizations can be realized with an excitatory coupling nor direct/conventional synchronizations can be realized with an inhibitory coupling as a result of the nature of the nonlinear function and the parametric relation obtained from the stability analysis using the Krasvoskii-Lyapunov stability theory. Numerical simulations are presented in confirmation with the experimental results and the transitions in the spectrum of Lyapunov exponents of the coupled time-delay systems also confirm the observed synchronization transitions.

The plan of the paper is as follows. In Sec. II, we present the details of the delay dynamical system under consideration and the experimental implementation of the system using an appropriate analog electronic circuit. Unidirectionally coupled time-delay system and its circuit details are discussed in Sec. III. In Sec. IV, we analyze the different synchronization manifolds and identify the conditions for the stability of the synchronized states of unidirectionally coupled time-delay systems. In Sec. V, we demonstrate experimentally the existence of anticipatory, complete, and lag synchronizations with excitatory coupling, and their inverse counterparts with inhibitory coupling are discussed in Sec. VI, along with their numerical confirmation. Finally in Sec. VII, we summarize our results.

II. THE SCALAR DELAYED CHAOTIC SYSTEM WITH THRESHOLD NONLINEARITY

We consider the following first-order time delay differential equation (DDE) describing the delay feedback oscillator,

$$\frac{dx}{dt} = -ax(t) + bf[x(t - \tau)], \qquad (1)$$

where a and b are positive parameters, $x(t)$ is a dynamical variable, $f(x)$ is a nonlinear activation function and τ
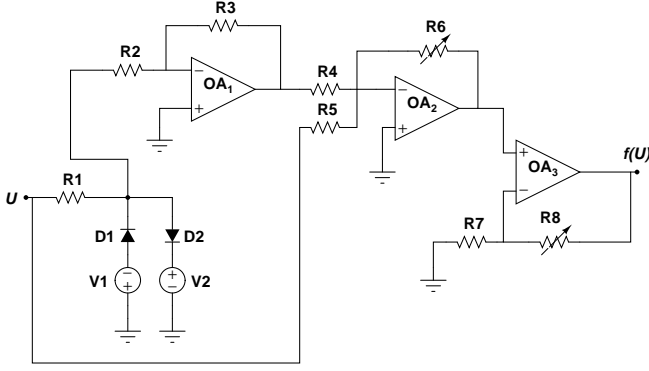
FIG. 3: Nonlinear device unit (ND): Circuit implementation of the nonlinear activation function with amplifying stages (OA_2, OA_3).
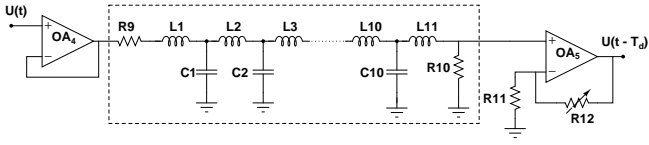

FIG. 4: Circuit implimentation of the time delay unit with a buffer (OA_4) and an amplifying stage (OA_5).

is the time delay. The function $f(x)$ is taken to be a symmetric piecewise linear function defined by [35]

$$f(x) = Af^* - Bx. \qquad (2a)$$

Here

$$f^* = \begin{cases} -x^* & x < -x^*, \\ x & -x^* \le x \le x^*, \\ x^* & x > x^* \end{cases} \qquad (2b)$$

where x^* is a controllable threshold value, and A and B are positive parameters. In our analysis, we chose $x^* = 0.7$, $A = 5.2$, $B = 3.5$, $a = 1.0$ and $b = 1.2$. It may be noted that for $|x| > x^*$, the function $f(x)$ has the negative slope $-B$ and it lies in all the four quadrants of the $f - x$ plane (Fig. 1(a)). The figure reveals the piecewise linear nature of the function. Experimental implementation (see below) of the function $f(x)$ is shown in Fig.1(b) in the form of voltage characteristic U_{in}vsU_{out} of the nonlinear device unit ND of Figs. 2 and 3.

This function $f(x)$ employs a threshold controller for flexibility. It efficiently implements a piecewise linear function. The control of this piecewise linear function facilitates controlling the shape of the attractors. Even for a small delay value this circuit system exhibits hyperchaos and can produce multi-scroll chaotic attractors by just introducing more number of threshold values, for example a square wave. In particular, this method is effective and simple to implement since we only need to monitor a single state variable and reset it if it exceeds the threshold and so has potential engineering applications for various chaos-based information systems.

A. Experimental setup

The system described by Eq. (1) with the nonlinear function $f(x)$ is constructed using analog electronic devices. The circuit (Fig. 2) has a ring structure and comprises of a diode based nonlinear device unit (Fig. 3) with amplifying stages (OA_2, OA_3), a time delay unit (Fig. 4) with a buffer (OA_4) and an amplifying stage (OA_5). The dynamics of the circuit in Fig. 2 is represented by a DDE of the form

$$R_0 C_0 \frac{dU(t)}{dt} = -U(t) + F[k_f U(t - T_d)], \qquad (3)$$

where $U(t)$ is the voltage across the capacitor C_0, $U(t - T_d)$ is the voltage across the delay unit (DELAY), T_d is the delay time and $F[k_f U(t - T_d)]$ is the static characteristic of the ND.

In order to analyze the above circuit, we transform it onto the dimensionless oscillator (1) on the basis of the following relations by defining the dimensionless variables and dimensionless parameters as

$$x(t) = \frac{U(t)}{U_s}, \quad \hat{t} = \frac{t}{R_0 C_0}, \quad \tau = \frac{T_d}{R_0 C_0}. \qquad (4)$$

A nonzero U_s is chosen such that $ND(U_s) = U_s$. In addition, the other parameters and variables are described by the relations $k_f = 1 + (\frac{R8}{R7}) = b$, $V1 = V2 = 0.7V$, $A = (R6/R4)$, $B = (R6/R5)$. These relations reveal that the circuit equation (3) is identical to Eq. (1) with $a = 1.0$. Without loss of generality, $\hat{t}$ is treated as t itself in our further analysis.

The approximate time delay T_D is given by

$$T_d = n\sqrt{LC}, \quad n \ge 1 \qquad (5)$$

where n is the number of LC filters in Fig. 4. The experimental circuit parameters are : $R1 = 1k\Omega$, $R2 = R3 = 10k\Omega$, $R4 = 2k\Omega$, $R5 = 3k\Omega$, $R6 = 10.4k\Omega$ (trimmer-pot), $R7 = 9.9k\Omega$, $R8 = 2.1k\Omega$ (trimmer-pot), $R9 = R10 = 1k\Omega$, $R11 = 10k\Omega$, $R12 = 20k\Omega$ (trimmer-pot), $R_0 = 2.68k\Omega$ (trimmer-pot), $C_0 = 100nF$, $L_i = 12mH(i = 1, 2, ..., 11)$, $C_i = 470nF(i = 1, 2, ..., 10)$, $n = 10$. From (5), we can see that $T_d = 0.751$ ms, $R_0 C_0 = 0.268$ ms, so that the time-delay $\tau \approx 2.8$ for the chosen values of the circuit parameters. The delay time can be simply varied by using the variable resistance R_0. In our circuit, $\mu A741s$ are employed as operational amplifiers. The constant voltage sources $V1$, and $V2$, and the voltage supply for all active devices are fixed at ± 12 Volts. The threshold value of the three segments involved in Eq. (2) can be altered by adjusting the values of voltages $V1$ and $V2$.

For the above choice of the circuit parameters, the values of the dimensionless parameters turns out to be $b = k_f = 1 + (\frac{R8}{R7}) \approx 1.212$, $A = (R6/R4) = 5.2$, $B = (R6/R5) \approx 3.467$ and the delay time $\tau = 2.8$.
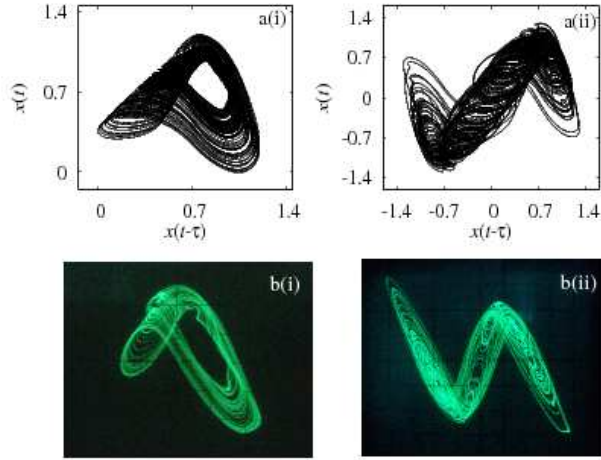
FIG. 5: (Colour online) (a) Phase portraits of chaotic attractors from Eqs. (1) and (2) for the parameters $a = 1, b = 1.2, A = 5.2, B = 3.5$ and $x^* = 0.7$: (i) one-band chaos for $\tau = 1.33$ and (ii) double-band chaos for $\tau = 2.8$. (b) Phase portraits of chaotic attractors from the circuit (Fig. 2), $U(t - T_d)$ against $U(t)$, vertical scale $2V/div.$, horizontal scale $0.2V/div.$: (i) one band chaos for $R_0 = 5640\ \Omega$ and (ii) double band chaos for $R_0 = 2680\ \Omega$.

B. Results

To start with, Eq. (1) has been numerically integrated with the chosen nonlinear function $f(x)$ for the parameter values $a = 1.0$, $b = 1.2$, $\tau = 2.8$, $x^* = 0.7$, $A = 5.2$, and $B = 3.5$, with the initial condition $x = 0.9$ in the range $t \in (-\tau, 0)$. A one-band chaotic attractor is shown in Fig. 5a(i) for $\tau = 1.33$, while for $\tau = 2.8$ a double-band hyperchaotic attractor is obtained (Fig. 5a(ii)). The corresponding experimental results are shown in Figs. 5b(i) and 5b(ii) for the values of the parameter $R_0 = 5640\Omega$ (in this case $\tau = T_d/R_0C_0 \approx 1.331$) and $R_0 = 2680\Omega$ (now $\tau = T_d/R_0C_0 \approx 2.8022$), respectively. The experimental results are in good agreement with the numerical ones and also in their corresponding parameter values.

The system described by Eqs. (1) and (2) exhibit multiple positive Lyapunov exponents for large values of the delay time, a typical feature of time-delay systems. The seven maximal Lyapunov exponents for the above parameter values as a function of the time-delay τ in the range $\tau \in (1, 10)$ are shown in Fig. 6, which are evaluated using the procedure of [36]. Now it is evident from the maximal Lyapunov exponents that the single band chaotic attractors shown in Figs. 5a(i) and b(i) for the value of delay time $\tau = 1.33$ and the resistance $R_0 = 5640\Omega$, respectively, has one positive Lyapunov exponent, while the double band chaotic attractor shown in Figs. 5a(ii) and b(ii) for the value of the delay time $\tau = 2.8$ and the resistance $R_0 = 2680\Omega$, respectively, has two positive Lyapunov exponents corroborating its hyperchaotic nature. We will demonstrate in the following sections the existence of different kinds of synchronization transitions
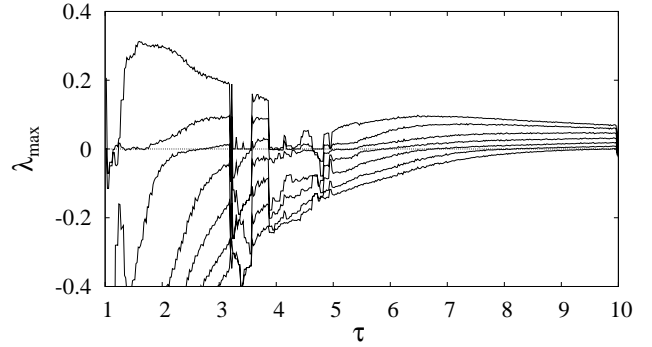

FIG. 6: The seven maximal Lyapunov exponents λ_{max} of the time-delay system (1) and (2) for the parameter values $a = 1$, $b = 1.2$, $x^* = 0.7$, $A = 5.2$, $B = 3.5$ and $\tau \in (1, 10)$.
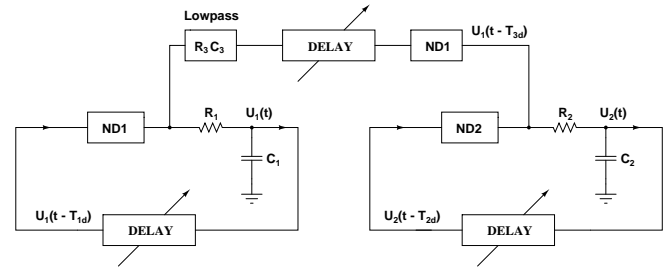

FIG. 7: Circuit block diagram of the coupled delayed feedback oscillator. Two delay oscillators are coupled through a nonlinear activation function (ND) but with a different time delay T_{3d} in the coupling with a low pass first-order R_3C_3 filter. $U_1(t)$ and $U_2(t)$ are the voltages across the capacitances C_1 and C_2, respectively. $U(t - T_{1d}) = U(t - T_{2d})$ are the voltages across the delay units of both the coupled oscillators.

in the hyperchaotic regime in coupled systems.

III. COUPLED TIME DELAY SYSTEMS WITH THRESHOLD NONLINEARITY

Now let us consider the following set of unidirectionally coupled first-order delay differential equations,

$$\frac{dx}{dt} = -a_1 x(t) + b_1 f\left[x(t - \tau_1)\right], \qquad (6a)$$

$$\frac{dy}{dt} = -a_2 y(t) + b_2 f\left[y(t - \tau_1)\right] + b_3 f\left[x(t - \tau_2)\right], \quad (6b)$$

where $a_1 = a_2 > 0$ are positive constants, $b_1 \neq b_2$ contributes to the parameter mismatch resulting in coupled non-identical systems, b_3 is the coupling strength, τ_1 is the feedback delay and τ_2 is the coupling delay. The nonlinear function $f(x)$ is of the same form as in Eq. (2).

Now to analog simulate the coupled time-delay systems (Eqs. (6)) and to demonstrate experimentally the existence of different types of synchronizations, a unidirectionally coupled time-delay electronic circuit is constructed as shown in the block diagram of Fig. 7. One

of the electronic oscillator circuits is used as the drive system, while the other structurally identical circuit is used as the response system with some parameter mismatches. The drive voltage ($U_1(t)$) after the delay line in the drive system is fed back to the nonlinear part (ND_1) of the drive system and a fixed R_1C_1 filter with time delay to generate chaotic/hyperchaotic oscillations. Similarly, the response circuit with a nonlinear part (ND_2), a delay line and a fixed R_2C_2 filter is capable of generating chaotic/hyperchaotic oscillations. The signal after the nonlinear function of drive is used as the transmission signal, which is unidirectionally transmitted through the lowpass filter (R_3C_3), delay line and nonlinear part to the response circuit. All the parameters need to be matched between the drive and the response circuits, whereas the parameters of the nonlinear activation functions of the drive, the response and the coupling are to be fixed according to the parametric relation obtained from the stability analysis (given below in Sec. IV).

The state equations of the coupled electronic circuit (Fig. 7) can be written as

$$R_1C_1 \frac{dU_1(t)}{dt} = -U_1(t) + f[k_{1f}U_1(t - T_{1d})], \qquad (7a)$$

$$\begin{aligned} R_2C_2 \frac{dU_2(t)}{dt} &= -U_2(t) + f[k_{2f}U_2(t - T_{2d})] \\ &\quad + f[k_{3f}U_1(t - T_{3d})], \end{aligned} \qquad (7b)$$

where the variables U_1 and U_2 correspond to the output variables of each circuit. By defining the new normalized variables as $x = \frac{U_1}{U_s}$, $y = \frac{U_2}{U_s}$, $\hat{t} = \frac{t}{R_1C_1}$, $\tau_1 = \frac{T_{1d}}{R_1C_1} = \frac{T_{2d}}{R_2C_2}$ and $\tau_2 = \frac{T_{3d}}{R_3C_3}$, one can check that the circuit equation (7) is identical to Eq. (6) with $a_1 = a_2 = 1.0$, $k_{1f} = b_1$, $k_{2f} = b_2$, $k_{3f} = b_3$ and $\hat{t} \to t$.

Before demonstrating the experimental results and the corresponding numerical confirmation of various synchronizations in the coupled time-delay systems (6) and (7), we deduce a *sufficient* stability condition, using the Krasovskii-Lyapunov theory, valid for different synchronization manifolds. After choosing the appropriate parameter values satisfying the obtained stability condition, we will demonstrate the existence of anticipatory, complete and lag synchronizations as a function of the coupling delay τ_2 for excitatory coupling and their inverse counterparts for inhibitory coupling in the same system both experimentally and numerically. It is to be noted that neither inverse synchronizations can be realized with excitatory coupling nor direct/conventional synchronizations can be realized with inhibitory coupling as a result of the nature of the nonlinear function and the parametric relation between b_1, b_2 and b_3 obtained from the stability analysis.

IV. SYNCHRONIZATION MANIFOLD AND ITS STABILITY CONDITION

Consider the direct synchronization manifold $\Delta = x_{\tau_2 - \tau_1} - y = 0$ of the coupled time-delay equation (6) with excitatory coupling $+b_3 f[x(t - \tau_2)]$, $b_3 > 0$, (correspondingly the inverse complete synchronization manifold becomes $\Delta = x_{\tau_2 - \tau_1} + y = 0$ with the inhibitory coupling $-b_3 f[x(t - \tau_2)]$, $b_3 > 0$, in Eq. (6b)), where $x_{\tau_2 - \tau_1} = x(t - (\tau_2 - \tau_1))$, which corresponds to the following distinct cases:

1. Anticipatory synchronization (AS) occurs when $\tau_2 < \tau_1$ with $y(t) = x(t - \hat{\tau}); \hat{\tau} = \tau_2 - \tau_1 < 0$, where the state of the response system anticipates the state of the drive system synchronously with the anticipating time $|\hat{\tau}|$. In contrast, in the case of the inverse anticipatory synchronization (IAS), the state of the response system anticipates exactly the inverse state of the drive system, that is, $y(t) = -x(t - \hat{\tau})$.

2. Complete synchronization (CS) results when $\tau_2 = \tau_1$ with $y(t) = x(t); \hat{\tau} = \tau_2 - \tau_1 = 0$, where the state of the response system evolves in a synchronized manner with the state of the drive system, while in the case of inverse complete synchronization (ICS), the state of the response system evolves exactly identical but inverse to the state of the drive system, that is, $y(t) = -x(t)$.

3. Lag synchronization (LS) occurs when $\tau_2 > \tau_1$ with $y(t) = x(t - \hat{\tau}); \hat{\tau} = \tau_2 - \tau_1 > 0$, where the state of the response system lags the state of the drive system in synchronization with the lag time $\hat{\tau}$. However, in the case of inverse lag synchronization (ILS), the state of the response system lags exactly inverse to the state of the drive system, that is, $y(t) = -x(t - \hat{\tau})$.

Now, the time evolution of the difference system with the state variable $\Delta = x_{\tau_2 - \tau_1} - y$ can be written for small values of Δ by using the evolution Eqs. (6) as

$$\begin{aligned} \dot{\Delta} &= \dot{x}_{\tau_2 - \tau_1} + \dot{y}(t) & (8) \\ &= -a\Delta + Af(x(t - \tau_2))[b_1 - b_2 - b_3] + b_2 A f'(x(t - \tau_2)) \times \\ &\quad \Delta_{\tau_1} - B x(t - \tau_2)[b_1 - b_2 - b_3] - b_2 B \Delta_{\tau_1}. & (9) \end{aligned}$$

The above inhomogeneous equation can be rewritten as a homogeneous equation of the form

$$\dot{\Delta} = -a\Delta + b_2[Af'(x(t - \tau_2)) - B]\Delta_{\tau_1}, \qquad (10)$$

for the specific choice of the parameters

$$b_1 = b_2 + b_3, \qquad (11)$$

so that the stability condition can be deduced analytically. The synchronization manifold corresponding

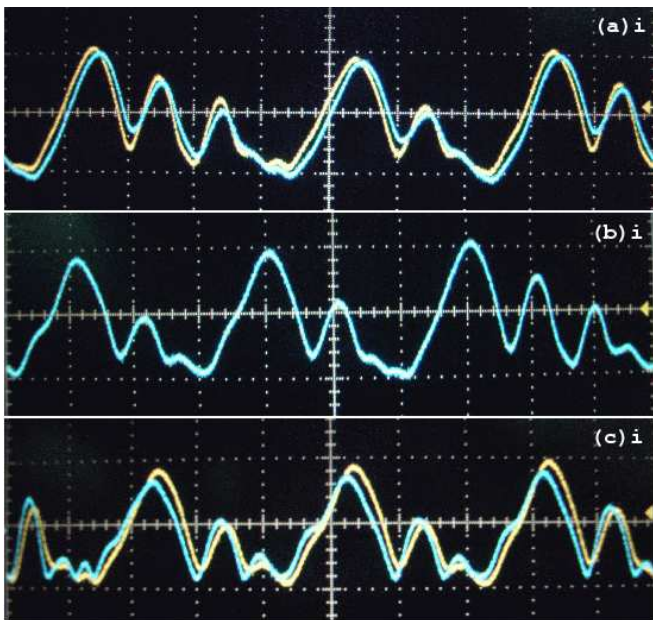FIG. 8: (Colour online) Experimental time series plot of the drive $U_1(t)$ (blue) and the response $U_2(t)$ (yellow), $\frac{T_{1d}}{R_1C_1} = \frac{T_{2d}}{R_2C_2} = \tau_1 \approx 2.8022$, $\frac{T_{3d}}{R_3C_3} = \tau_2$, $C_1 = C_2 = C_3 = 100\ nF$, $R_1 = R_2 = 2680\ \Omega$ and $T_{1d} = T_{2d} = T_{3d} = 0.751$ ms (a) anticipatory synchronization for $R_3 = 3004\ \Omega$ (now $\tau_2 \approx 3.1007$), (b) complete synchronization for $R_3 = 2680\ \Omega$ (now $\tau_2 \approx 2.8022$) and (c) lag synchronization for $R_3 = 2422\ \Omega$ (now $\tau_2 = 2.5$); vertical scale $5V/div.$, horizontal scale $1ms$.

to Eq. (10) is locally attracting if the origin of the above error equation is stable. Following the Krasovskii-Lyapunov functional approach [27, 37], we define a positive definite Lyapunov functional of the form

$$V(t) = \frac{1}{2}\Delta^2 + \mu \int_{-\tau_1}^{0} \Delta^2(t+\theta)d\theta, \qquad (12)$$

where μ is an arbitrary positive parameter, $\mu > 0$.

The above Lyapunov function, $V(t)$, approaches zero as $\Delta \to 0$. Hence, the required solution $\Delta = 0$ to the error equation, Eq. (10), is stable only when the derivative of the Lyapunov functional $V(t)$ along the trajectory of Eq. (10) is negative. This requirement results in the condition for stability as

$$\Gamma(\mu) = 4\mu(a-\mu) > b_2^2\left[Af'(x(t-\tau_2)) - B\right]^2. \qquad (13)$$

Again $\Gamma(\mu)$ as a function of μ for a given $f'(x)$ has an absolute minimum at $\mu = \left[|b_2(Af'(x(t-\tau_2)) - B)|\right]/2$ with $\Gamma_{min} = |b_2(Af'(x(t-\tau_2)) - B)|$. Since $\Gamma \geq \Gamma_{min} = |b_2(Af'(x(t-\tau_2)) - B)|$, from the inequality (13), it turns out that a *sufficient* condition for asymptotic stability is

$$a > |b_2(Af'(x(t-\tau_2)) - B)|. \qquad (14)$$

Now from the form of the piecewise linear function $f(x)$ given by Eq. (2), we have,

$$|f'(x(t-\tau_2))| = \left\{ \begin{array}{ll} 0, & |x| > x^* \\ 1.0, & |x| \leq x^* \end{array} \right. \qquad (15)$$

Consequently the stability condition (14) becomes $a > |b_2(A-B)| > |b_2B|$ along with the parametric relation $b_1 = b_2 + b_3$. Since the deduced stability condition is independent of the delay times τ_1 and τ_2, the same general stability condition is valid for anticipatory, complete and lag synchronizations with excitatory coupling and to their inverse counterparts with inhibitory coupling.

We remark here that if one substitutes $y \to \hat{y} = -y$ in Eq. (6b), then the excitatory coupling becomes an inhibitory coupling and the inhibitory coupling becomes an excitatory coupling due to the nature of the nonlinear function, $f(x)$. Furthermore, one obtains the parametric relation $b_2 = b_1 + b_3$ along with the same stability condition (14) for both the cases of excitatory coupling with an inverse synchronization manifold and inhibitory coupling with a direct synchronization manifold. Therefore, to obtain both direct and inverse synchronizations either from excitatory or from inhibitory coupling both the parametric relations, that is $b_2 = b_1 + b_3$ and $b_1 = b_2 + b_3$ given by (11), have to be satisfied for fixed values of the nonlinear parameters b_1 or b_2 and for positive values of the coupling strength b_3. The only way to satisfy both the parametric relations and the stability condition, $a > |b_2(A-B)| > |b_2B|$, is to choose negative values for the coupling strength b_3 and this changes the nature of the coupling. Hence, one cannot obtain inverse (anticipatory, complete and lag) synchronizations with excitatory coupling or direct (anticipatory, complete and lag) synchronizations with inhibitory coupling for the chosen form of the unidirectional nonlinear coupling due to the nature of the parametric relation (11) and the stability condition (14).

V. DIRECT SYNCHRONIZATIONS WITH EXCITATORY COUPLING

In this section, we will demonstrate the existence of anticipatory, complete and lag synchronizations as a function of the coupling delay τ_2, both experimentally and numerically, for the choice of the parameters satisfying the stability condition (14) for the case of excitatory coupling.

A. Anticipatory Synchronization

For $\tau_2 < \tau_1$, the synchronization manifold $\Delta = x_{\tau_2-\tau_1} - y = 0$ becomes an anticipatory synchronization manifold as described above. We have fixed the value of the feedback delay $\tau_1 = 2.8$ and the coupling delay $\tau_2 = 2.5$, while the other parameters are fixed as $a = 1.0$,
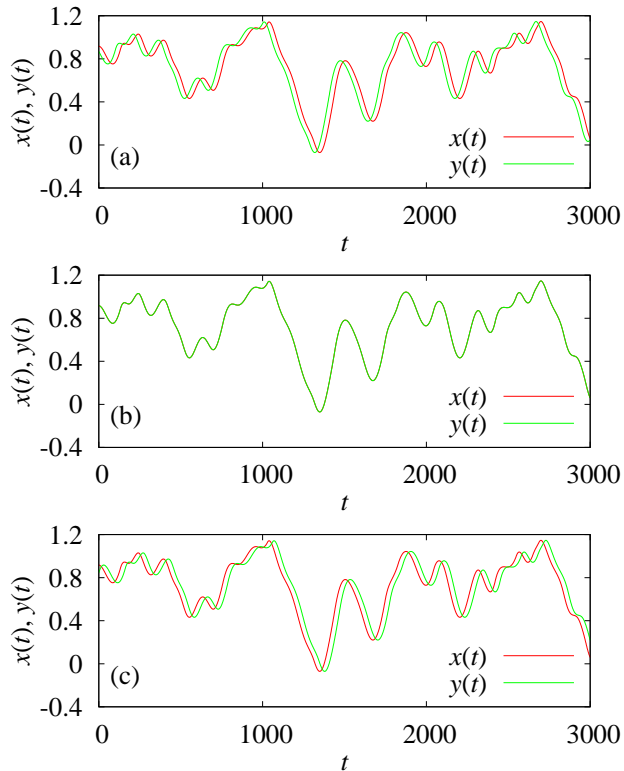
FIG. 9: (Colour online) Numerical time series plots of the drive $x(t)$ and the response $y(t)$ systems for the parameter values $a_1 = a_2 = 1.0, b_1 = 1.2, b_2 = 0.58, b_3 = 0.62, A = 5.2, B = 3.5, x^* = 0.7$ and $\tau_1 = 2.8$: (a) anticipatory synchronization for $\tau_2 = 2.5$, (b) complete synchronization for $\tau_2 = 2.8$ and (c) lag synchronization for $\tau_2 = 3.1$.

$b_1 = 1.2$, $x^* = 0.7$, $A = 5.2$, and $B = 3.5$. The value of the nonlinear parameters are fixed as $b_2 = 0.58$ and $b_3 = 0.62$ such that both the stability condition (14) and the parametric relation (11) are satisfied. All the above parameter values are fixed to be the same except for the coupling delay τ_2 for the remaining part of the study. The experimental and the numerical time series plots of both the drive $x(t)$ and the response $y(t)$ systems are shown in Figs. 8a and 9a, respectively, for $\tau_2 < \tau_1$ demonstrating the existence of anticipatory synchronization. Both the experimental and the numerical phase space plots corresponding to the anticipatory synchronization manifold of the drive and the response systems are shown in Figs. 10(a)i and 10(a)ii, respectively.

The seven largest Lyapunov exponents of the coupled time-delay systems are shown in Fig. 11a as a function of the nonlinear parameter b_2 for the anticipatory synchronization manifold. For the values of delay times $\tau_1 = 2.5$ and $\tau_2 = 2.8$ the uncoupled systems exhibit only two positive Lyapunov exponents as may be seen from Fig. 6. The two positive Lyapunov exponents of the drive system remain positive, while one of the positive Lyapunov exponents of the response system becomes negative at

$b_2 \approx 0.9$ and the second positive Lyapunov exponent becomes negative at $b_2 \approx 0.7$ confirming the existence of exact anticipatory synchronization for $b_2 < 0.7$. It is to be noted that the Lyapunov exponents of the coupled systems indicate the existence of exact anticipatory synchronization also in the range $b_2 \in (0.7, 0.58)$ in which the stability condition (14) is not satisfied confirming that it is only a sufficiency condition but not a necessary one.

B. Complete Synchronization

For $\tau_2 = \tau_1$, the synchronization manifold $\Delta = x_{\tau_2-\tau_1} - y = 0$ becomes a complete synchronization manifold $\Delta = x(t) - y(t) = 0$. Now, we have fixed the value of the coupling delay as $\tau_2 = \tau_1 = 2.8$ for fixed values of the other parameters as mentioned in the previous section. The experimental and the numerical time series plots of both the drive $x(t)$ and the response $y(t)$ systems are shown in Figs. 8b and 9b, respectively, demonstrating the existence of complete synchronization between the coupled time-delay systems. The phase space plots of both the systems corresponding to the complete synchronization manifold are shown in Figs. 10b. The seven largest Lyapunov exponents (Fig. 11b) of the coupled time-delay systems corresponding to the complete synchronization manifold indicate that both the positive Lyapunov exponents of the response system become negative for $b_2 < 0.7$, while the two Lyapunov exponents of the drive system remain positive, confirming the existence of complete synchronization between the drive and response systems. Note that the coupled systems remain in a hyperchaotic state, that is, this transition to complete synchronization is a transition from one hyperchaotic regime to another one.

C. Lag Synchronization

The synchronization manifold $\Delta = x_{\tau_2-\tau_1} - y = 0$ becomes a lag synchronization manifold for $\tau_2 = 3.1 > \tau_1 = 2.8$. Both the time series and the phase space plots of the coupled time-delay systems obtained using our experimental realization are shown in Figs. 8c and 10(c)i, respectively, and those obtained using numerical simulations are shown in Figs. 9c and 10(c)ii, respectively, indicating the existence of a lag synchronization. Again, the seven largest Lyapunov exponents of the coupled time-delay systems shown in Fig. 11c for the lag synchronization manifold confirm the existence of it for $b_2 < 0.7$.

VI. INVERSE SYNCHRONIZATIONS WITH INHIBITORY COUPLING

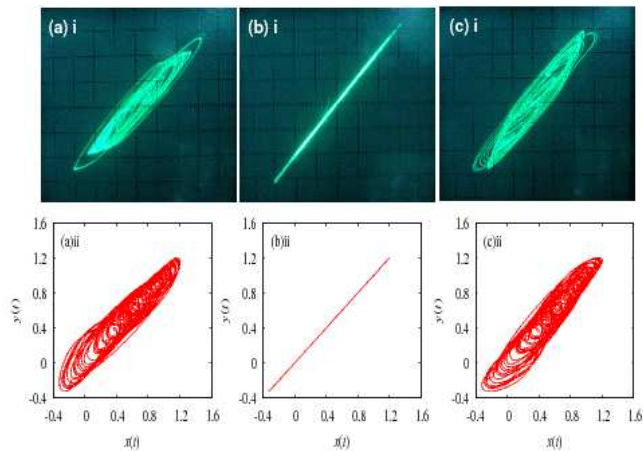Now we consider the inhibitory coupling, $-b_3 f[x(t - \tau_2)]$, in Eq. (6b) instead of the excita-

FIG. 10: (Colour online) Phase space plots of the drive $x(t)$ and the response $y(t)$: (a) anticipatory synchronization, (b) complete synchronization and (c) lag synchronization. Here the top panels correspond to experimental results for the same values of the parameters as in Fig. 8 and the bottom panels represent numerical results for the same values of the parameters as in Fig. 9.
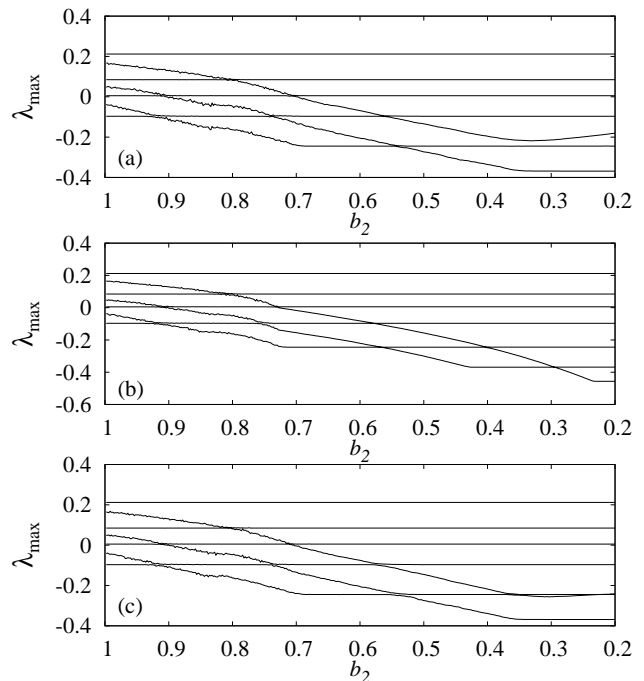

FIG. 11: The seven largest Lyapunov exponents of the coupled time-delay systems (6) for the same values of parameters as in Fig. 9 for (a) anticipatory synchronization manifold, (b) complete synchronization manifold and (c) lag synchronization manifold.

tory coupling $+b_3 f[x(t-\tau_2)]$ to demonstrate the transition from inverse anticipatory to inverse lag synchronization via an inverse complete synchronization as a function of the coupling delay τ_2 for the same values of parameters as in the Sec. V.

A. Inverse anticipatory synchronization

As discussed above, the inverse synchronization manifold $\Delta = x_{\tau_2-\tau_1} + y = 0$ becomes an inverse anticipatory synchronization manifold for $\tau_2 < \tau_1$. For the same values of all the parameters as in Sec. V A, the coupled time-delay system (6) exhibits an inverse anticipatory synchronization in the presence of inhibitory coupling as shown in Figs. 12a and 13a. The experimental and numerical phase plots of the coupled time-delay system corresponding to the inverse anticipatory synchronization manifold are shown in Figs. 14(a)i and 14(a)ii, respectively. The seven largest Lyapunov exponents of the coupled systems corresponding to the inverse anticipatory synchronization manifold are shown in Fig. 15a as a function of the nonlinear parameter b_2. The two largest positive Lyapunov exponents of the drive system remain unaltered in their values, while that of the response system become negative for $b_2 < 0.7$ confirming the existence of inverse anticipatory synchronization between the coupled time-delay systems with inhibitory coupling.

B. Inverse complete synchronization

An inverse complete synchronization manifold is obtained for $\tau_2 = \tau_1$. The time series plot of both the drive

and the response variables obtained from experimental realization are depicted in Fig. 12b and those obtained from numerical simulation are shown in Fig. 13b illustrating the existence of inverse complete synchronization. The experimental and numerical phase space plots of the coupled time-delay systems corresponding to the inverse complete synchronization manifold are depicted in Figs. 14(b)i and 14(b)ii, respectively. The seven largest Lyapunov exponents of the coupled time-delay systems (Fig. 15) confirm the existence of inverse complete synchronization indicated by a change in the signs of both the positive Lyapunov exponents of the response system for $b_2 < 0.7$, while that of the drive system remain unchanged.

C. Inverse lag synchronization

Again, for $\tau_2 > \tau_1$, the synchronization manifold $\Delta = x_{\tau_2-\tau_1} + y = 0$ becomes an inverse lag synchronization manifold. The experimental and the numerical time series plots, indicating the existence of inverse lag synchronization, of both the drive and response systems are shown in Figs. 12c and 13c, respectively. The corresponding phase space (of inverse lag synchronization) plots are also depicted in Figs. 14(c)i and 14(c)ii, respectively. The seven largest Lyapunov exponents of the
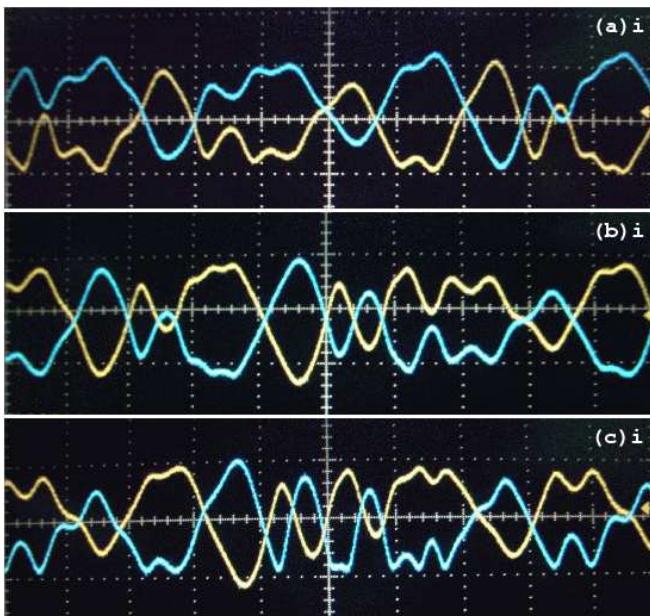
FIG. 12: (Colour online) Experimental time series plots of the drive $U_1(t)$ (blue) and the response $U_2(t)$ (yellow), $\frac{T_{1d}}{R_1 C_1} = \tau_1$, $\frac{T_{2d}}{R_2 C_2} = \tau_1$, $\frac{T_{3d}}{R_3 C_3} = \tau_2$, $C_1 = C_2 = C_3 = 100$ nF, $R_1 = R_2 = 2680$ Ω and $T_{1d} = T_{2d} = T_{3d} = 0.751$ ms: (a) inverse anticipatory synchronization for $R_3 = 3004$ Ω, (b) inverse complete synchronization for $R_3 = 2680$ Ω and (c) inverse lag synchronization for $R_3 = 2422$ Ω; vertical scale $5V/div.$, horizontal scale $1ms/div$

coupled time-delay systems corresponding to inverse lag synchronization manifold are shown in Fig. 15c again as a function of b_2. The two positive Lyapunov exponents of the drive system remain positive, while that of the response system become negative for $b_2 < 0.7$ confirming the existence of inverse lag synchronization between the coupled time-delay systems.

VII. SUMMARY AND CONCLUSION

In this paper, we have presented experimental observations of typical kinds of synchronization transitions in a system of unidirectionally coupled piecewise-linear time-delay electronic circuit designed using a threshold controller. In particular, we have shown the transition from anticipatory synchronization to lag synchronization through complete synchronization and their inverse counterparts with excitatory and inhibitory couplings, respectively, as a function of the coupling delay and for a fixed set of other parameters. A common stability condition valid for all these synchronized states is deduced and it is independent of both the feedback and the coupling delays. Futher, experimental observations are confirmed by numerical simulations and also from transitions in the Lyapunov exponents of the coupled time-delay systems. We also note that the nature of the piecewise linear func-
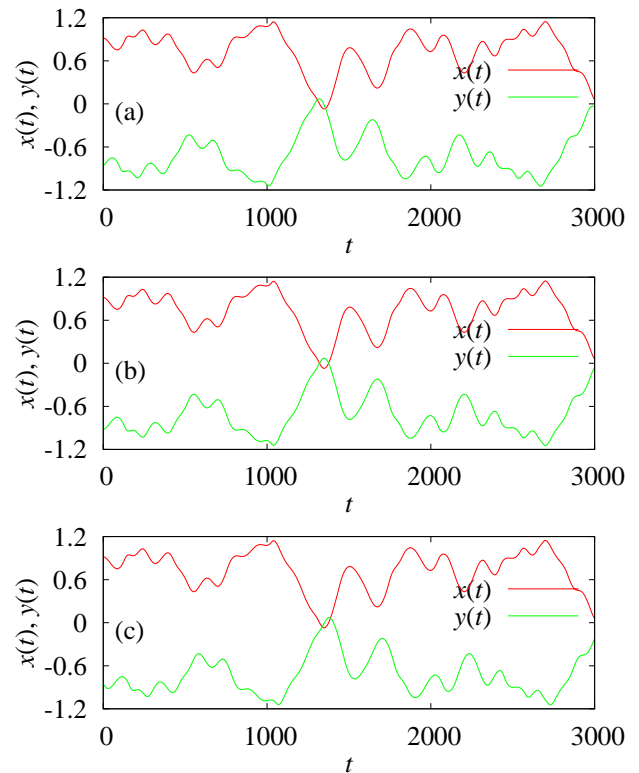

FIG. 13: (Colour online) Numerical time series plots of the drive $x(t)$ and the response $y(t)$ systems for the parameter values $a_1 = a_2 = 1.0, b_1 = 1.2, b_2 = 0.58, b_3 = 0.62, A = 5.2, B = 3.5, x^* = 0.7$ and $\tau_1 = 2.8$: (a) inverse anticipatory synchronization for $\tau_2 = 2.5$, (b) inverse complete synchronization for $\tau_2 = 2.8$ and (c) inverse lag synchronization for $\tau_2 = 3.1$.
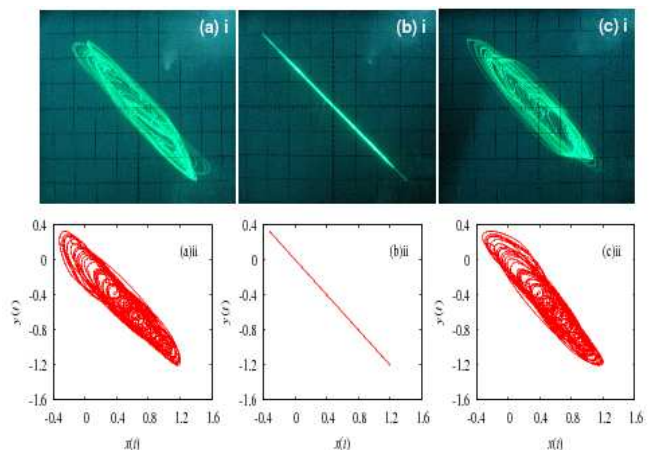

FIG. 14: (Colour online) Phase space plots of the drive $x(t)$ and the response $y(t)$ for the same parameter values as in Figs. 9 and 8: (a) inverse anticipatory synchronization for $\tau_2 = 2.5$, (b) inverse complete synchronization for $\tau_2 = 2.8$ and (c) inverse lag synchronization for $\tau_2 = 3.1$.
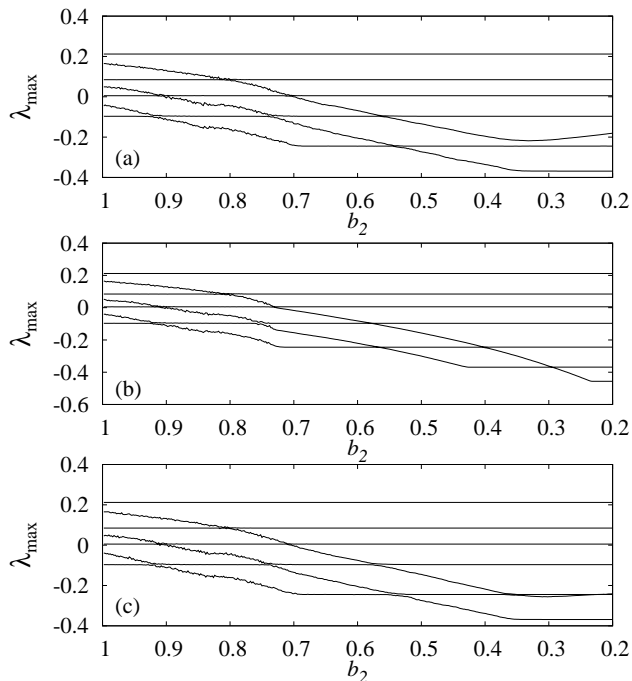
FIG. 15: The seven largest Lyapunov exponents of the coupled time-delay systems (6) for the same values of parameters as in Fig. 9 for (a) inverse anticipatory synchronization manifold, (b) inverse complete synchronization manifold and (c) inverse lag synchronization manifold.

tion in the proposed circuit can be easily changed by using multiple threshold values and that multi-scroll hyperchaotic attractors can also be produced even for a small value of delay time for further study and applications.

Acknowledgments

[1] S. Kim, S. H. Park, and C. S. Ryu, Phys. Rev. Lett. **79**, 2911 (1997).

[2] D. V. Ramana Reddy, A. Sen, and G. L. Johnston, Phys. Rev. Lett. **85**, 3381 (2000).

[3] G. C. Sethia, A. Sen, and F. M. Atay, Phys. Rev. Lett. **100**, 144102 (2008).

[4] A. Prasad, J. Kurths, S. K. Dana, and R. Ramaswamy, Phys. Rev. E **74**, 035204(R) (2006).

[5] F. M. Atay, J. Jost, and A Wende, Phys. Rev. Lett. **92**, 144101 (2004).

[6] C. Masoller, and A. C. Marti, Phys. Rev. Lett. **94**, 134102 (2005).

[7] M. Dhamala, V. K. Jirsa, and M. Ding, Phys. Rev. Lett. **92**, 074104 (2004).

[8] A. Argyris, D. Syvridis, L. Larger, V. Annovazzi-Lodi, P. Colet, I. Fischer, J. Garcia-Ojalvo, C. R. Mirasso, L. Pesquera, and K. A. Shore, Nature **438**, 343 (2005).

[9] M. A. Dahlem, F. M. Schneider, and E. Schöll, Chaos **18**, 026110 (2008).

[10] F. M. Schneider, E. Schöll, and M. A. Dahlem, Chaos **19**, 015110 (2009).

[11] S. Sivaprakasam, I. Pierce, P. Rees, P. S. Spencer, K. A. Shore,and A. Valle, Phys. Rev. A **64**, 013805 (2001).

[12] I. Wedekind, and U. Parlitz, Phys. Rev. E **66**, 026218 (2002).

[13] M. Peil, T. Heil, I. Fischer, and W. Elsässer, Phys. Rev. Lett. **88**, 174101 (2002).

[14] Y. Liu, Y. Takiguchi, P. Davis, T. Aida, S. Saito, and J. M. Liu, Appl. Phys. Lett. **80**, 4306 (2002).

[15] A. Uchida, K. Higa, T. Shiba, S. Yoshimori, F. Kuwashima, and H. Iwasawa, Phys. Rev. E **68**, 016215 (2003).

[16] A. Uchida, S. Kinugawa, T. Matsuura, and S. Yoshimori, Phys. Rev. E **67**, 026220 (2003).

[17] I. Fischer, R. Vicente, J. M. Buldu, M. Peil, C. R. Mirasso, M. C. Torrent, and J. Garcia-Ojalvo, Phys. Rev. Lett. **97**, 123902 (2006).

[18] J. M. Buldu, T. Heil, I. Fischer, M. C. Torrent, and J. Garcia-Ojalvo, Phys. Rev. Lett. **96**, 024102 (2006).

[19] A. Englert, W. Kinzel, Y. Aviad, M. Butkovski, I. Reidler, M. Zigzag, I. Kanter, and M. Rosenbluh, Phys. Rev. Lett. **104**, 114102 (2010).

[20] S. Sivaprakasam, E. M. Shahverdiev, P. S. Spencer,and K. A. Shore, Phys. Rev. Lett. **87**, 154101 (2001).

[21] S. Tang, and J. M. Liu, Phys. Rev. Lett. **90**, 194101 (2003).

[22] H. U Voss, Int. J. Bifurcation and Chaos **12**, 1619 (2002).

[23] S. Sano, A. Uchida, S. Yoshimori, and R. Roy, Phys. Rev. E **75**, 016207 (2007).

[24] M.-Y. Kim, C. Sramek, A. Uchida, and R. Roy, Phys. Rev. E **74**, 016211 (2006).

[25] A. Wagemakers, J. M. Buldú, and M. A. F. Sanjuán, Europhys. Lett. **81**, 40005 (2008); Chaos **17**, 023128 (2007).

[26] D. V Senthilkumar, M. Lakshmanan, and J. Kurths,

Phys. Rev. E **74**, 035205(R) (2006).

[27] D. V Senthilkumar, and M. Lakshmanan, Phys. Rev. E **71**, 016211 (2005).

[28] D. V Senthilkumar, J. Kurths, and M. Lakshmanan, Phys. Rev. E **79**, 066208 (2009); Chaos **19**, 023107 (2009).

[29] H. U Voss, Phys. Rev. E **61**, 5115 (2000); H. U Voss, Phys. Rev. Lett. **87**, 014102 (2001).

[30] C. Masoller, Phys. Rev. Lett. **86**, 2782 (2001).

[31] C. Masoller, and D. H. Zanette, Physica A (Amsterdam) **300**, 359 (2001).

[32] M. Zhan, G. W. Wei, and C. H. Lai, Phys. Rev. E **65**, 036202 (2002).

[33] I. Belykh, and A. Shilnikov, Phys. Rev. Lett. **101**, 078102 (2008).

[34] S. Jalil, I. Belykh, and A. Shilnikov, Phys. Rev. E **81**, 045201(R) (2010).

[35] K. Srinivasan, I. Raja Mohamed, K. Murali, M. Lakshmanan, and S. Sinha, Int. J. Bifurcation and Chaos (submitted) , (2010).

[36] J. D. Farmer, Physica D **4**, 366 (1982).

[37] N. N. Krasovskii, *Stability of Motion* (Stanford University Press, Stanford, 1963); K. Pyragas, Phys. Rev. E **58**, 3067 (1998).